THE JOURNAL OF COMPARATIVE NEUROLOGY 499:49–63 (2006)

Differential Expression of Muscarinic Acetylcholine Receptors Across Excitatory and Inhibitory Cells in Visual Cortical Areas V1 and V2 of the Macaque Monkey

ANITA A. DISNEY,* KUNAL V. DOMAKONDA, AND CHIYE AOKI
[1]Center for Neural Science, New York University, New York, New York 10003

ABSTRACT

Cholinergic neuromodulation, a candidate mechanism for aspects of attention, is complex and is not well understood. Because structure constrains function, quantitative anatomy is an invaluable tool for reducing such a challenging problem. Our goal was to determine the extent to which m1 and m2 muscarinic acetylcholine receptors (mAChRs) are expressed by inhibitory vs. excitatory neurons in the early visual cortex. To this end, V1 and V2 of macaque monkeys were immunofluorescently labelled for γ-aminobutyric acid (GABA) and either m1 or m2 mAChRs. Among the GABA-immunoreactive (ir) neurons, 61% in V1 and 63% in V2 were m1 AChR-ir, whereas 28% in V1 and 43% in V2 were m2 AChR-ir. In V1, both mAChRs were expressed by fewer than 10% of excitatory neurons. However, in V2, the population of mAChR-ir excitatory neurons was at least double that observed in V1. We also examined m1 and m2 AChR immunoreactivity in layers 2 and 3 of area V1 under the electron microscope and found evidence that GABAergic neurons localize mAChRs to the soma, whereas glutamatergic neurons expressed mAChRs more strongly in dendrites. Axon and terminal labelling was generally weak. These data represent the first quantitative anatomical study of m1 and m2 AChR expression in the cortex of any species. In addition, the increased expression in excitatory neurons across the V1/V2 border may provide a neural basis for the observation that attentional effects gain strength up through the visual pathway from area V1 through V2 to V4 and beyond. J. Comp. Neurol. 499:49–63, 2006.

Indexing terms: cholinergic; neuromodulation; GABAergic; striate cortex; immunofluorescence; electron microscopy; ultrastructure; dual labelling

Cholinergic neuromodulation is essential not only for cognitive processes (Rezvani and Levin, 2001; Sarter et al., 2003) but also for the sensory processing upon which cognition depends (Metherate and Weinberger, 1989; Sato et al., 1987; Sillito and Kemp, 1983; Stone, 1972b; Wozniak et al., 1989). Acetylcholine (ACh) is synthesized by neurons in the basal forebrain and released in all parts of the neocortex (Mesulam et al., 1983a,b). In the cortex, ACh is released from terminals to bind at receptors distant from synaptic specializations (Aoki and Kabak, 1992; de Lima and Singer, 1986; Descarries et al., 1997; Mrzljak et al., 1995; Smiley et al., 1997; but see Turrini et al., 2001; Umbriaco et al., 1994). In volume transmission such as this, knowing which cell types express ACh receptors (AChRs) is critical, because it is in the receiving that a nonsynaptic signal becomes specific. One of the simplest ways to classify neuronal cell types is according to their primary neurotransmitter substance, which in the primary visual cortex of macaques is either glutamate or γ-aminobutyric acid (GABA) for at least 95% of neurons (for review see DeFelipe, 1993). It has long been known that many glutamatergic neurons in mammalian cortex

Grant sponsor: National Institutes of Health; Grant number: R01-NS41091 (to C.A.); Grant number: R01-EY13145 (to C.A.); Grant number: P30-EY13079 (to C.A. and J. Anthony Movshon).

*Correspondence to: Anita Disney, Center for Neural Science, NYU, 4 Washington Place, Room 809, New York, NY 10003.
E-mail: anita@nyu.edu

Received 8 March 2006; Revised 27 April 2006; Accepted 9 May 2006
DOI 10.1002/cne.21096
Published online in Wiley InterScience (www.interscience.wiley.com).

express muscarinic AChRs and are modulated by acetylcholine acting at these receptors (Hasselmo and Bower, 1992; McCormick and Prince, 1985, 1986; Stone, 1972a,b; Wang and McCormick, 1993). Evidence also exists for cholinergic modulation of cortical GABAergic interneurons. In cat visual cortex, cholinergic varicosities are often juxtaposed to GABA-immunoreactive somata (Beaulieu and Somogyi, 1991; Erisir et al., 2001) and ACh's suppressive/hyperpolarising effects can be blocked by application of bicuculline, both in vitro (McCormick and Prince, 1986) and in vivo (Muller and Singer, 1989). Furthermore, in vitro evidence from layer 5 of rat sensory cortex shows that nicotine and muscarine directly affect distinct subpopulations of GABAergic neurons in different ways (Xiang et al., 1998). Despite these data showing that both excitatory and inhibitory neurons are targets for ACh, most models of cholinergic modulation in cortex focus explicitly or implicitly on modulation of excitatory neurons (see, e.g., Hasselmo and McGaughy, 2004; Linster and Cleland, 2002; Linster et al., 2003; Yu and Dayan, 2005).

There is evidence for diverse and complex cholinergic effects in cortex; however, extracellular physiology cannot distinguish effects on excitation from those on inhibition, and many in vitro (intracellular) studies record exclusively from pyramidal neurons. Thus the extent to which ACh's observed effects result in modulation of inhibition vs. excitation remains unclear. There are no quantitative anatomical data comparing AChR expression across cell types, and there are few anatomical data at all on cholinergic receptor expression in one of the most heavily studied and best understood cortical model systems, the primary visual cortex (area V1) of the macaque monkey.

There are five mammalian genes coding for distinct mAChRs (S.V.P. Jones, 1993). Among these, the m1 and m2 AChRs are known to be strongly expressed in the neocortex of monkeys (Mrzljak et al., 1993; Tigges et al., 1997) and represent the two pharmacological classes of muscarinic receptor (pirenzepine sensitive, or M1 class, and pirenzepine insensitive, or M2 class). There is also evidence that m2 AChR expression may differ across functional compartments in vision (Mrzljak et al., 1996).

Although there are good qualitative data on ACh receptor (AChR) localization in macaque cortex already (Han et al., 2000; Mrzljak et al., 1993; Tigges et al., 1997), we provide the first quantitative study of m1 and m2 muscarinic receptors in this, or in any, species. We combine antibodies directed against these mAChRs with one directed against the inhibitory neurotransmitter GABA in a dual-immunofluorescence study. Because roughly one in five neurons in layers 2–6 of V1 is GABAergic (Beaulieu et al., 1992; Fitzpatrick et al., 1987), if AChRs were distributed evenly across the whole population of neurons (excitatory and inhibitory), cells dually labelled for GABA and an AChR should account for 20% of all AChR-immunoreactive cells. Instead, we find that more than 50% of mAChR-expressing neurons in V1 are GABAergic. We also report that this proportion drops to 25–35% in area V2, suggesting a different role for cholinergic modulation between these two apparently similar early visual areas.

MATERIALS AND METHODS

Tissue preparation

Animals. Two adult (3.6 and 3.1 kg) male cynomologous monkeys (*Macaca fascicularis*) were used in the immunofluorescence experiments for this study, and two adult (4.2 and 4.9 kg) male rhesus macaques (*Macaca mulatta*) were used in the immunoelectron microscopic experiments. Unfixed tissue from three additional animals (all *fascicularis*) was used for Western blot control experiments for testing antibody selectivity. All animals had been used previously for unrelated electrophysiological experiments, the *fascicularis* for acute recordings (Solomon et al., 2004) and the *mulatta* for chronic (awake-behaving) experiments (Platt and Glimcher, 1997). All procedures were approved by the Institutional Care and Use Committee for New York University, in accordance with the guidelines of the National Institutes of Health.

Histological preparation. Animals were euthanized by i.v. injection of sodium pentobarbital (65 mg/kg). After EEG-determined brain death (*fascicularis*) or complete abolition of corneal and pedal reflexes (*mulatta*), animals were transcardially perfused with heparinized lactated Ringer followed by 4 liters of chilled, freshly prepared 4% paraformaldehyde with 0.1% (*mulatta*) or 0.25% (*fascicularis*) glutaraldehyde. The fixative was run for at least 40 minutes. The visual cortex was blocked and removed by a coronal cut at the level of the lunate sulcus and postfixed overnight at 4°C in 4% paraformaldehyde. On the following day, the entire block was vibratome-sectioned at a thickness of 40 μm in the sagittal plane and reacted for 30 minutes in 1% sodium borohydride in 0.1 M PB (pH 7.4) to stop further glutaraldehyde fixation. After 0.1 M PB rinses, every third section was set aside to make up a cytochrome oxidase reference set. The remaining sections were stored at 4°C in 0.01 M phosphate-buffered saline (PBS; pH 7.4) with .05% sodium azide added.

Cytochrome oxidase histochemistry. Cytochrome oxidase histochemistry (Wong-Riley et al., 1998) was commenced no more than 72 hours after perfusion. Sections were preincubated at 4°C in a solution of 4% sucrose in 0.1 M PB, on a shaker, then transferred into 0.1 M PB with 4.5% (w/v) sucrose, 0.02% catalase (Sigma, St; Louis, MO), 0.03% cytochrome C (Sigma), and 0.05% 3,3′-diaminobenzidine HCl (Aldrich, Milwaukee, WI) and placed in a shaker oven. Maintained at between 37°C and 39°C, the tissue was incubated for up to 48 hours, with refreshed solution after the first 24 hours, until cytochrome oxidase blobs were clearly visible in layers 2 and 3. After rinses in 0.1 M PB, the sections were mounted, counterstained for Nissl bodies, and coverslipped for permanent storage and viewing under the light microscope.

GABA/AChR dual immunofluorescence labelling

Immunocytochemistry. Sections were randomly selected from the remaining tissue (after removal of sections for making the reference set) from both of the cynomologous monkeys. A freeze-thaw technique was used to improve antibody penetration (Wouterlood and Jorritsma-Byham, 1993). The tissue was cryoprotected in a series of 10-minute washes through 5%, 10%, and 20% dimethylsulfoxide (DMSO) in 0.1 M PB, then run through eight freeze-thaw cycles, each comprising a brief dip in partially frozen isopentane, followed by a thaw in room temperature 20% DMSO. The tissue was then rinsed in PBS before being placed in a blocking solution of 1% IgG-free bovine serum albumin (BSA; Molecular Probes, Eugene, OR) and 0.05% sodium azide in 0.01 M PBS for 30 minutes.

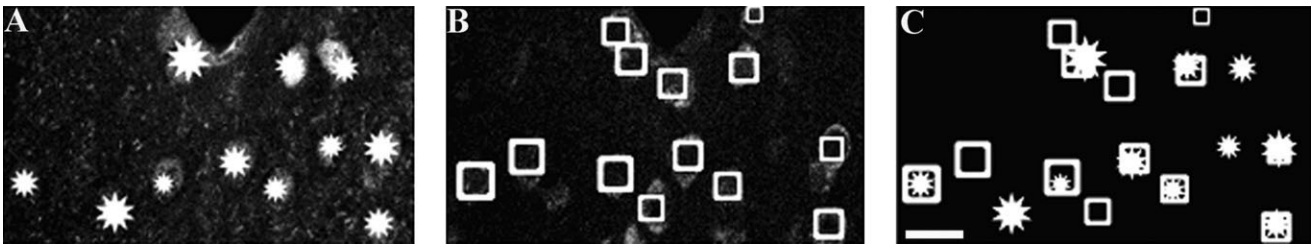

Fig. 1. Illustration of counting method. **A** shows the isolated "red" channel, representing GABA immunoreactivity. Stars have been drawn on top of immunoreactive somata. Marking of images was done in gray scale, as the images appear here. In **B**, squares have been used in a similar fashion to indicate the location of somata immunoreactive for the m1 AChR. Counting was from images like that shown in **C**, in which the data-containing channels have been turned off. Stars alone would be counted as singly labelled for GABA (here 3), squares alone as m1 AChR single-label (here 5), and a star inside a square shows the presence of a dually labelled soma (8). Scale bar = 50 μm.

The primary antibodies were diluted in the above-described blocking solution. Free-floating sections were exposed to two antibodies (an anti-GABA plus one anti-AChR) in a single coincubation step. A polyclonal rabbit anti-m1 receptor antibody (1:200; directed against amino acids 227–353 of the i3 intracellular loop; Chemicon, Temecula, CA; catalog No. AB5164, lots 22060712 and 22060716) or a polyclonal rabbit anti-m2 receptor antibody (1:200; directed against amino acids 225–356 of the i3 intracellular loop; Chemicon; catalog No. AB5166, lot 22051030) were combined with a monoclonal mouse anti-GABA (1:100; directed against purified GABA; Sigma; catalog No. A0310, lot 042K4817). The tissue was incubated in these antibodies for 72 hours at room temperature on a shaker.

After the primary incubation and PBS rinses, the tissue was incubated with secondary antibodies, diluted 1:50 in blocking solution. All secondary antibodies were raised in chicken. GABA-ir sites were always visualized with the Alexa 594 nm fluorophore (Alexa 594 chicken anti-mouse IgG; Molecular Probes; catalog No. A21201, lot 84C1), whereas, for AChR-ir sites, we used the Alexa 488 fluorophore (Alexa 488 chicken anti-rabbit IgG; Molecular Probes; catalog No. A-21441, lot 93C1). This second incubation proceeded in the dark, at room temperature, for 4–6 hours. The sections were then briefly rinsed in PBS, mounted, and dried overnight in the dark before coverslipping. Slides were stored in the dark at 4°C.

Confocal microscopy. Data were collected from the opercular surface of V1 (2–8° parafoveal visual field representation), from inside the calcarine sulcus (V1 representation of the peripheral visual field), and from dorsal region of the posterior bank of the lunate sulcus (parafoveal V2). Data for all the three regions (parafoveal V1, peripheral V1 and V2) were collected from the same tissue section. This was done to ensure that the immunolabelling within the regions to be compared was obtained under identical conditions.

With a Zeiss LSM 310 confocal microscope, image montages running from the pia to the white matter were collected with a ×63 objective and stored for off-line analysis. Each image covered a 200-μm × 200-μm × <0.25-μm (z-axis resolution estimated by Abbe's equation) region of tissue. Additional images were taken at depths between 600 and 1,200 μm from the pial surface in area V1, to ensure adequate sampling of the thin layers 4A and 4B. A low-magnification reference section of the photobleached region of tissue was taken with a ×10 objective after each montage to enable coregistration with the relevant cytochrome oxidase reference section.

Determining layer boundaries using cytochrome oxidase reference sections. For each immunolabelled section, an adjacent 40-μm cytochrome oxidase reference section was used to identify laminar boundaries. Digital images were taken of the reference sections with a ×10 objective, focusing on the region of neuropil adjacent (in the "z axis") to each data montage. Coregistration of the fluorescence and light microscopic images was achieved using gross section morphology, pial surface shape, artefacts, and blood vessels as fiduciary marks. The depths, in micrometers from the pial surface, of layers 4A, 4B, 4C, 5, and 6 of area V1 and layers 4, 5, and 6 of area V2 were recorded on the reference images. These measurements were then converted to the magnification of the data images and the layer boundaries drawn on each image along with a ±7.5-μm confidence boundary. The depth of the boundary between layer 1 and layer 2 was determined by eye based on the sharp increase in the density of cell somata at the layer transition, as visualized under the confocal microscope.

Counting labelled cells in fluorescence data images. Labelled somata were counted in Adobe Photoshop 6.0. Data channels (red and green) were isolated and identified somata counted separately from gray-scale images. Only wholly visible somata were marked for counting, and those that crossed either the image boundary or the 15-μm confidence boundary around layer borders were excluded. The cell body was marked with a shape that reflected the soma size, drawn in a separate Photoshop image layer. Cell counts were made from the drawn shapes, with the red and green (data) channels turned off. Both single- and double-labelled GABA/AChR-ir cells were counted. For a cell to be counted as dually labelled, the markings for soma size and location had to be precisely matched. This is shown in Figure 1, in which stars are used to mark GABA-ir cells (Fig. 1A) and squares are used to show the location of m1 ACh-ir neurons (Fig. 1B). In Figure 1C, a star inside a square indicates a dually labelled neuron. In cases in which these markings overlapped but appeared to differ in location and/or size, the red and green channels were turned back on, and a qualitative determination was made. Less than 1% of the sample required this additional qualitative determination (none in the example shown in Fig. 1).

Immunoelectron microscopy: immunocytochemistry

The sections used for electron microscopy were processed as part of an unrelated tract-tracing study involving injections of BDA into the lateral geniculate nucleus of two rhesus macaques. Sections from V1 of both animals were chosen for processing based on the presence of strong terminal field labelling layer 4C in an adjacent reference section. Again, the freeze-thaw technique was used to improve antibody penetration (see dual immunofluorescence protocol described above for details). After this procedure, and after 30 minutes at room temperature in 1% hydrogen peroxide in PBS to block endogenous peroxidases, the tissue was rinsed in PBS before being placed in a blocking solution of 1% IgG-free bovine serum albumin (BSA; Molecular Probes) with 0.05% sodium azide (Sigma), 0.04% Triton X-100 (Triton), and 0.1% Photoflo (Kodak) in 0.01 M PBS for 30 minutes. The same mAChR antibodies as were used in the immunofluorescence experiments (m1 and m2; both from Chemicon) were diluted (1:200) in PBS with 1% BSA and 0.05% sodium azide. Free-floating sections were incubated in these primary antibodies for 72 hours at room temperature on a shaker.

The silver-intensified immunogold method was used for visualization. After the primary incubation and PBS rinsing, the tissue was incubated overnight at room temperature in a 0.8-nm gold-conjugated goat anti-rabbit IgG, diluted 1:50 in PBS with 1% BSA and 0.05% sodium azide.

On the next day, after brief PBS rinses, the sections were postfixed with 2% glutaraldehyde in PBS for 10 minutes and then rinsed again before silver enhancement. After three brief washes in 0.2 M citrate buffer (pH 6.5) to remove the PBS, the gold particles were enlarged by immersing sections in silver solution for up to 12 minutes, with the Amersham IntenSE silver enhancement kit (with refreshed silver solution if more than 6 minutes was required). The silver enhancement was followed by citrate buffer and then 0.1 M phosphate buffer rinses.

The tract-tracing study necessitated a further step (visualizing the tracer) not actually needed for the current data collection. Briefly, after the silver autometallography, sections were incubated overnight in avidin-horseradish peroxidase solution (Vector ABC Elite; Vector, Burlingame, CA) diluted in PBS, to detect a biotinylated dextran-amine tracer substance. On the next day, 3,3′-diaminobenzidine HCl (DAB) with hydrogen peroxide as a substrate for the HRP was used to visualize the tracer.

The now dually labelled sections were rinsed in 0.1 M PB and fixed with 0.5% osmium tetroxide in 0.1 M PB for 30 minutes, followed by dehydration in 50% ethanol and an overnight incubation in 4% uranyl acetate in 70% ethanol at 4°C on a shaker. On the next day, the dehydration series proceeded through 70%, 90%, and 100% ethanol and three 30-minute acetone rinses before overnight infiltration of 1:1 Embed 812 (EM Sciences, Fort Washington, PA)/acetone and then 100% Embed 812. After being embedded in Epon capsules and 48 hours of curing at 60°C, the tissue was resectioned at a thickness of 80–90 nm, mounted on formvar-coated nickel grids, and counterstained with Reynold's lead citrate. The grids were then ready for inspection and data collection under a JEOL 1200 XL transmission electron microscope.

Data collection

Data for the EM study were collected from images of layers 2 and 3 taken as part of complete pia to white matter montages. Images were taken at ×40,000. To ensure that we sampled tissue within the region of antibody penetration, these montages did not run perfectly perpendicular to the pial surface but instead traced the interface between the tissue and the embedding resin. The micrographs were taken using Kodak monochrome negatives and were printed on Kodak paper.

Reference images at ×120 were taken after each session on the electron microscope. The path of the electron beam is visible in these images and was used as an aid in coregistering the image montages with a series of reference images. The reference images comprised a micrograph of the same section taken with a ×10 objective on a light microscope; a series of camera lucida drawings made of the resin-embedded tissue with ×4, ×10, and ×20 objectives; and micrographs of an adjacent cytochrome oxidase reference section.

Each data image overlapped very slightly with the immediately preceding image, allowing accurate tracking of depth from the pial surface. Regions of overlap were marked off and counted only once during data collection. The depth of laminar boundaries was measured on ×40 images of the adjacent cytochrome oxidase reference section. Neuronal profiles were counted if they contained one or more silver particles. This permissive criterion was adopted because there were low overall levels of immunoreactivity, accompanied by a very low level of nonspecific labelling, as assessed by the complete absence of silver particles visible on the myelin sheaths of axons.

Antibody controls

Primary antibodies. The generation of the i3 loop fusion proteins and antibodies used in this study has been described elsewhere (Levey et al., 1991). The specificity of these antibodies has been tested in rodent by immunoprecipitation (Levey et al., 1991) and by immunohistochemistry in m1 (Hamilton et al., 1997) or m2 (Duttaroy et al., 2002) AChR knockout mice. In addition, we have run controls to ensure specificity of action in nonhuman primate tissue. First, controls were run for nonspecific binding with preadsorbed antibodies. The antigens used for preadsorption were identical to the immunogens used in synthesis of the antibodies, comprising the target peptide sequence on the i3 loop (amino acids 227–353 for m1 and 225–356 for m2) conjugated to a GST fusion protein. The antibody and antigen (3–6 μg of blocking peptide per 1 μg of antibody, peptide provided by the antibody manufacturer; Chemicon) were coincubated for 2 hours at 32°C (diluted in the PBS/BSA/azide blocking solution). The solution was centrifuged at 20,000*g* for 30 minutes and the supernatant used in an ABC-DAB visualization protocol (Hsu et al., 1981). Briefly, after incubating sections in blocking solution for 30 minutes and then in the preadsorbed antibody (diluted 1:500) for 72 hours, the sections were rinsed and transferred into a biotinylated goat anti-rabbit IgG antibody solution (1:100; Vector). After 1 hour in the secondary antibody, the sections were again rinsed and then incubated for 30 minutes in a solution containing an avidin-HRP conjugate (ABC Elite; Vector). The antigenic sites were visualized at the LM level, with hydrogen peroxide and 3,3′-diaminobenzidine HCl as a substrate for

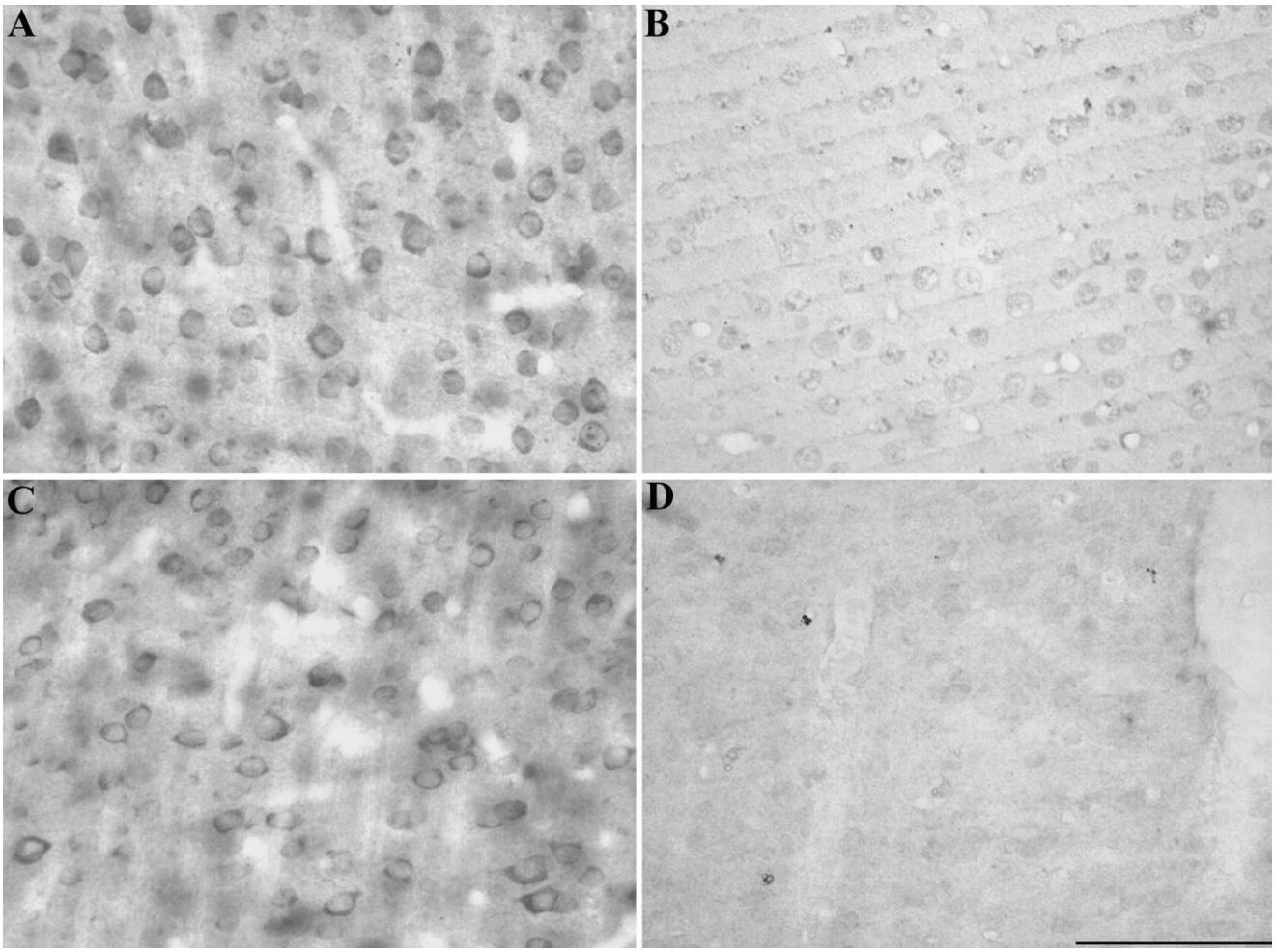

Fig. 2. Preadsorption control on V1 tissue. The micrographs at left show immunoreactivity in area V1 for the m1 (**A**) and m2 (**C**) AChRs, visualized by an ABC-DAB reaction. **B** and **D** show the preadsorption controls for m1 and m2, respectively. The same concentration of primary antibody has been used (1:500 in both cases), but the antibody has been preadsorbed against a saturating concentration of a synthetic peptide identical to the immunogen used in creating each antibody. For the m1 AChR, this peptide represents amino acids 227–353 of the human m1 AChR; for m2, it is amino acids 225–356, also of the human receptor. The only digital image correction performed on this figure was to *increase* the contrast for both images on the right (from the preadsorbed tissue) to reveal the tissue edges. Scale bar = 50 μm.

the HRP. Preadsorption abolished the vast majority of the immunolabelling (Fig. 2B,D).

Western blotting. Samples of V1 (unfixed) were taken from three anesthetized male cynomologous monkeys. Small blocks of tissue were removed with an ice-cold scalpel and either immediately homogenized or frozen on dry ice and stored at −80°C. Samples were homogenized in 12% sucrose (w/v), 0.5% EGTA, 0.8% EDTA, 0.4% sodium orthovanadate, and 20% protease inhibitor cocktail (Sigma) on ice and then centrifuged at 10,000*g*, and the supernatant was stored at −80°C. Protein content of the homogenate was determined by using Lowry's method.

Homogenates were run on a 7.5% SDS-polyacrylamide gel (Bio-Rad, Hercules, CA) and transferred to nitrocellulose paper for Western blotting. After preincubation for 1 hour in the Western blotting buffer, consisting of PBS with 0.1% Tween-20 (PBS-T), 5% dry milk, and 0.025% sodium azide for 1 hour, the nitrocellulose paper was incubated overnight at 4°C in the Western blotting buffer containing one or the other of the primary antibodies (anti-m1 AChR 1:150; anti-m2 AChR 1:200) or in a preadsorbed primary antibody, prepared as described above under Primary antibodies. After thorough rinsing in PBS-T, the nitrocellulose was incubated in an HRP-conjugated secondary antibody (1:50,000; Jackson Immunoresearch, West Grove, PA) for 1 hour. The labelled bands were visualized by a chemiluminescent (ECL Plus; Amersham, Arlington Heights, IL) signal on X-ray film (Kodak X-Omat AR). The molecular weight of each immunolabelled band was estimated based on a marker run in the immediately adjacent lane (33–200 kD Rainbow Marker reference proteins; Bio-Rad). Each antibody produced a band at ~78 kD (Fig. 3B,E), the expected molecular weight of the receptors (Venter, 1983). In a manner that appeared to depend on the duration of heating samples prior to loading the gel, receptor dimers (at approxi-

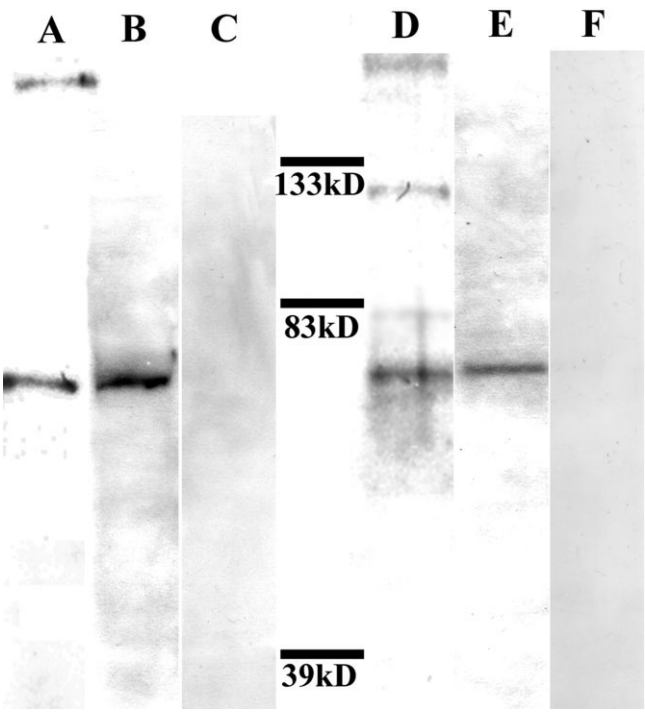

Fig. 3. Western blots controls for m1 and m2 AChR antibodies. Western blots were run for both the m1 and the m2 AChR antibodies. The Kodak X-Omat AR film was scanned on an Epson scanner. **A–C** show data for the anti-m1 AChR antibody. **D–F** show data for the anti-m2 AChR antibody. In B (m1 AChR) and E (m2 AChR), a single band can be seen at the expected weight for these muscarinic receptors (60–80 kD). In A (m1) and D (m2), this same band can be seen, along with additional bands at double and triple weight. These additional bands result from processing-dependent oligomerization. Preadsorption (C,F) of the antibodies abolished these bands. B and D have been altered to remove scratches on the film. The contrast of C and F has been increased to aid visibility.

mately double this weight, shown in Figure 3D for the m2 receptor) and trimers (observed for both receptors, Fig. 3A,D) were sometimes seen, as has been reported previously (Chemicon technical data sheet; Park and Wells, 2004). The ~78-kD band was eliminated by antibody preadsorption (Fig. 3C,F).

Secondary antibodies. Avian host (chicken) secondaries were chosen to minimize cross-reactivity with mammalian IgGs. Additionally, the secondaries were preadsorbed against IgGs from the nontarget host animal. Specifically, the chicken anti-rabbit IgG that was used to detect the rabbit anti-mAChRs was preadsorbed against mouse IgG to avoid cross-reaction with the mouse anti-GABA. Similarly, the chicken anti-mouse IgG (used to detect the mouse anti-GABA) was preadsorbed against rabbit IgG to prevent it binding to the rabbit anti-mAChRs.

Controls for all secondary antibodies were included with each batch of processing in which both primary antibodies were omitted from solution used for the initial 72-hour incubation. In these controls, the tissue was incubated either in PBS with 1% BSA and 0.05% sodium azide only or in this buffer with normal rabbit serum added (both conditions included with each batch). In addition, we conducted a control experiment in which one or the other of the primary antibodies was omitted from the first incubation, but both secondaries were included at the second incubation step (i.e., one of the secondaries had no target epitope in the tissue and thus produced no fluorescent signal).

Statistical analysis

ANOVAs and *t*-tests were used as appropriate to analyze the data from the immunofluorescence study. Statistics were calculated in GraphPad's Prism (v4.0) software and checked by hand. Statistical analysis, though offered in this paper, is problematic when dealing with small samples. Our sample of neurons (>10,000) is very large, but our number of animals is very small (two). Data were originally collected from a third animal, but this monkey was perfused with 1% glutaraldehyde, which resulted in reduced m2 AChR immunoreactivity and variable patterns of m1 AChR labelling. This tissue gave qualitatively similar, but highly variable, results. The data from the remaining two animals show very little variability (see, e.g., Fig. 5), so it was decided to proceed with analyzing just their data. Exact *P* values are reported in the text.

RESULTS

Our goal was to determine the extent to which m1 and m2 AChRs were expressed by inhibitory vs. excitatory neurons in the early visual cortex of macaque monkeys. We used dual immunofluorescence and found that in V1 both types of mAChR were strongly expressed by inhibitory neurons but only weakly expressed by excitatory neurons. We also found that expression in excitatory cells increased across the V1/V2 border.

Greater than expected mAChR expression by GABAergic neurons in V1

The most reliable way to identify inhibitory neurons was to use an immunolabel for GABA, because mAChR immunoreactivity did not provide sufficient morphological information for accurate classification. For example, it can be seen in Figure 4 that some AChR-ir neurons appeared to have pyramidal somata (Fig. 4A, asterisks) but turned out to be GABA-ir (Fig. 4B). In addition, excitatory cells in layer IVC are stellate and have small somata, making them very difficult to distinguish reliably from their GABAergic neighbors. Figure 4 also illustrates the lack of bleed-through between channels in our data images; in one channel (the green) only the somatic cytoplasm is visible and in the other (red) only the nucleus.

Data were analyzed in terms of both the proportion of GABAergic interneurons expressing each mAChR and the proportion of AChR-ir neurons that was GABAergic. Because ~20% of V1 neurons are GABAergic (Hendry et al., 1987; Beaulieu et al., 1992), if AChRs were expressed proportionally across cell types, then roughly 20% of AChR-ir neurons in V1 should be dually labelled for GABA. However, we found that >50% of cells immunoreactive for each mAChR were GABAergic. GABA-ir neurons made up 60% of m1 AChR-ir (1,092 of 1,833, sd = 7%, *t*-test comparison against 20%, $P = 0.04$) and 52% of m2 AChR-ir (925 of 1,790, sd = 8%; *t*-test comparison against 20%, $P = 0.05$) neurons across all layers in V1. In fact, in every layer, the observed proportion of AChR-ir cells that

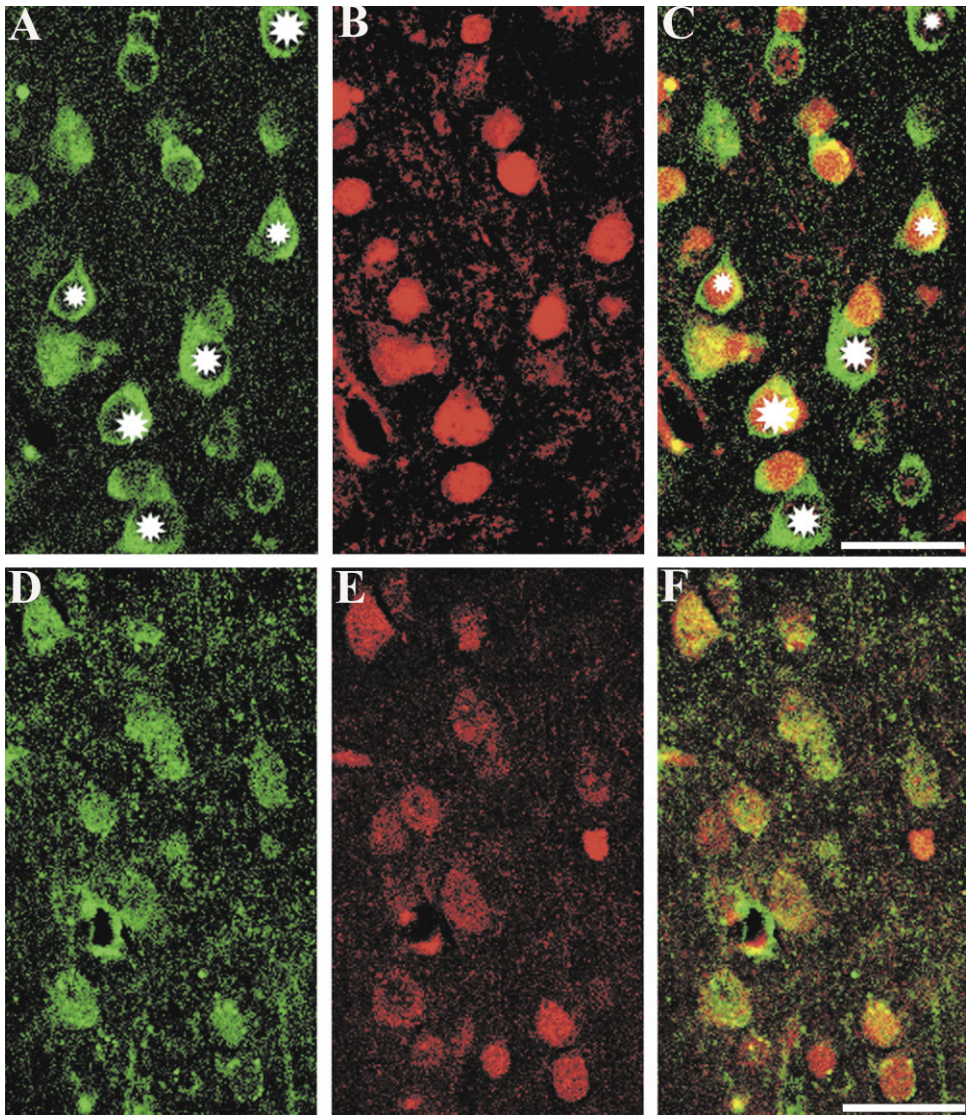

Fig. 4. Dual immunofluorescence for GABA and m1/m2 AChRs in V1. **A–C** show m1 AChR immunoreactivity, GABA immunoreactivity, and merged images taken from layer 3 of V1. **D–F** show m2 AChR, GABA, and merged images taken from layer 2 of V1. The green channel carries the signal representing m1 (A) or m2 (D) receptor immunoreactivity. The red channel (B,E) shows GABA immunoreactivity. In the merged images (C,F), dual labelling appears yellow. A shows a representative immunoreactivity profile for m1 AChRs in V1. The paucity of immunoreactive dendrites makes morphological characterization difficult. The stars over some of the labelled somata in A and C indicate cells that we might count as pyramidal neurons based on morphology, yet a number of these cells express GABA (B). In D, it is challenging to parcel labelled somata into "pyramidal" and "nonpyramidal" categories at all. Note also the absence of bleed-through between channels, the lack of nuclear red in the green channel, and the absence of any signal in the red channel from any of the bright green mAChR-ir somata. Scale bars = 25 μm.

was also GABA-ir far exceeded 20% (there were no differences between layers as assessed by a repeated-measures ANOVA), which clearly indicates enriched expression of both muscarinic receptors subtypes in GABAergic interneurons in macaque V1 (Fig. 5).

Overall, when all V1 neurons (GABA-ir and GABA-immunonegative) are considered, a relatively small population expresses mAChRs. Although the proportion of the GABA-ir population expressing m1 and m2 AChRs was high; 61% of GABAergic cells were m1 AChR-ir (1,092 of 1,792, sd = 6%) and 28% were m2 AChR-ir (925 of 3,356, sd = 8%; Fig. 6); those GABAergic cells account only for approximately 20% of all V1 neurons. Thus m1 AChR-expressing GABAergic neurons represent about 12% of all neurons in V1. However, this is over half of the m1 AChR-expressing population (60% of m1 AChR-expressing cells were interneurons), which suggests that only 20% of the neurons in V1 express m1 receptors and that only ~10% of glutamatergic neurons are m1 AChR-ir. By similar calculations, ~6% of V1 neurons are m2 AChR-expressing GABAergic interneurons, and this is half of the m2 AChR-ir population, so approximately 12% of V1 neurons express m2 AChRs, again indicating that less than 10% of glutamatergic cells are m2 AChR expressing (see Fig. 7).

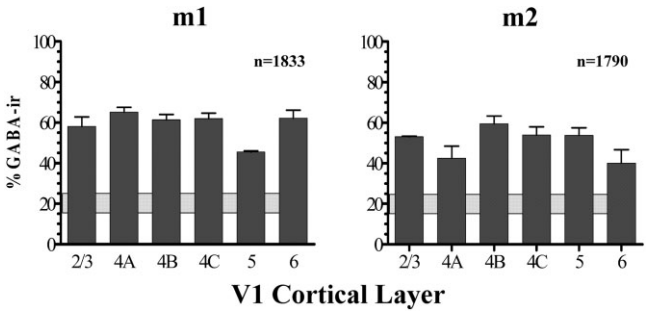

Fig. 5. Dually labelled cells among the mAChR-ir population in V1. These graphs show the percentages of mAChR-ir somata, in each layer of V1 (with the exception of layer 1), that were also immunoreactive for GABA, m1 AChR on the left, m2 AChR on the right. The solid line behind the bars in both graphs represents the expected value (20–25%) if the composition of the AChR-expressing population reflected the neuronal composition of macaque V1 (~80% glutamatergic, 20% GABAergic). For both receptors, in every layer, the observed value is well above this level, suggesting enriched expression of cholinergic receptors among cortical GABAergic neurons in macaque V1. N = 3,623 AChR-ir neurons; error bars show standard error.

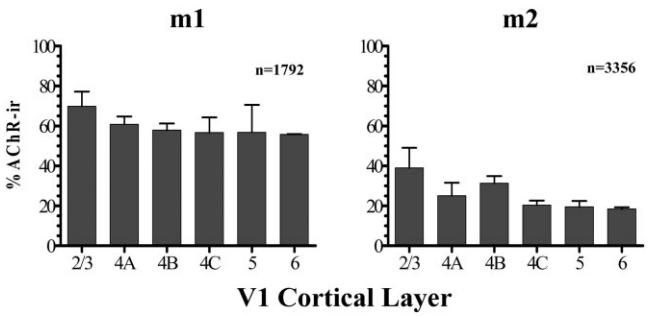

Fig. 6. Dually labelled cells among the GABA-ir population in V1. These graphs show the percentages of GABA-ir somata in each layer that were also immunoreactive for a muscarinic receptor (m1 AChRs on the left, m2 AChRs on the right). There is an even level of expression of both types of mAChR by interneurons across the cortical layers, with perhaps a trend toward increased expression in the upper layers. Among these two receptor subtypes, the m1 AChR is clearly the more strongly expressed. N = 5,148 GABA-ir neurons; error bars show standard error.

Electron microscopic localization of muscarinic receptors in V1

It is possible that the low observed levels of mAChR expression resulted from having chosen to quantify somatic labelling. To confirm these data, electron microscopy (EM) was used. EM provides easier-to-identify compartments and precise antigen localization. Neuronal profiles (i.e., excluding glia) were counted in images of m1 or m2 AChR-immunolabelled tissue taken from V1 (layers 2 and 3 only) of two macaque monkeys (different animals from those used in the immunofluorescence study; see Materials and Methods). The images were not randomly selected; rather, they comprised a continuous montage through layers 2 and 3, following the interface between tissue and embedding resin, this being the region penetrated by the antibodies. The data were also not randomly sampled within images; *all* neuronal profiles in each micrograph were counted. This resulted in a different sample

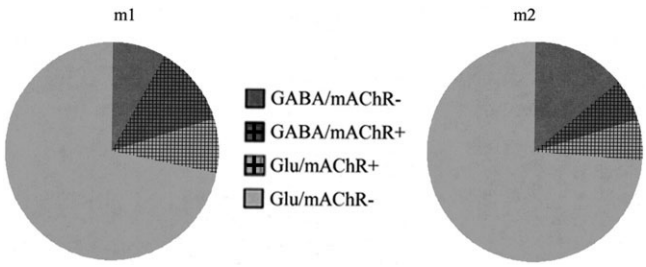

Fig. 7. Estimated mAChR expression by GABAeric and non-GABAergic cells in V1. These pie charts provide a graphic representation of our estimates for mAChR expression by GABAergic and glutamatergic neurons in V1. In both, the textured overlay shows the proportions of neurons that were immunoreactive for m1 (left, 20%) or m2 (right, 12%) AChRs. The solid gray circle behind this overlay represents all cortical neurons, with GABAergic neurons (20% of the population) in dark gray and glutamatergic neurons (80%) in pale gray. Most V1 neurons were not labelled by either marker (the untextured, pale grey region in each pie) indicating that they were glutamatergic neurons that did not expression m1 or m2 AChRs.

size for each profile type, reflecting the neuropil composition of the area.

The immunofluorescence (somatic) data showed that about 20% of all V1 cells (GABAergic or glutamatergic) express m1 AChRs and 12% express m2 AChRs. We counted 5,176 profiles in EM tissue processed for m1 AChR immunoreactivity and 3,987 profiles in the m2 AChR-processed tissue. The highest level of expression for both mAChRs was in dendrites; 25% (112 of 441) of all dendrites were m1 AChR-ir, and 12% (48 of 397) of all dendrites were immunoreactive for m2 AChRs. These values are highly comparable to the expression level observed for somata. For no cellular compartment (spines, dendrites, axons, terminals) did the proportion of immunolabelled elements suggest that the somatic count performed in the immunofluorescence study had underestimated the m1 and m2 AChR-expressing populations in V1 (Table 1).

It could still be argued, however, that both the EM and the fluorescence data reflect a tendency for GABAergic neurons to localize mAChRs to the soma, whereas glutamatergic neurons express their mAChRs elsewhere, out in the dendrites and axons. To explore this possibility, dendrites were separated based on their morphology, and mAChR expression was reexamined.

Dendritic labelling. GABAergic neurons have few, if any, spines and so receive their excitatory inputs directly onto shafts (glutamatergic neurons receive excitatory synapses onto spines), so, if a dendrite receives direct asymmetric (putatively glutamatergic) synapses onto the shaft itself (Fig. 8B,C), then that dendrite is likely to be part of a GABAergic neuron (White, 1989). Among 77 putatively GABAergic dendrites (with asymmetric synapses), only 19% (15 of 77) were m1 AChR-ir. This is substantially lower than the proportion of GABA-ir somata expressing m1 AChRs (61%). Similarly, only 13% (7 of 52) dendrites with asymmetric synapses were m2 AChR-ir (compared with 28% of somata). These data suggest a preferential somatic (vs. dendritic) localization of mAChRs on interneurons.

It is not possible to identify glutamatergic dendrites morphologically, unless the plane of section fortuitously contains the dendrite connected via a spine neck to a spine

TABLE 1 mAChR-ir Profiles in Layers 2 and 3[1]

	m1				m2			
	Terminals	Axons	Spines	Dendrites	Terminals	Axons	Spines	Dendrites
Layer 2	14 (257)	79 (2,131)	23 (168)	101 (309)	8 (294)	51 (2,380)	9 (227)	35 (311)
Layer 3	5 (219)	11 (1,813)	2 (97)	11 (132)	1 (78)	20 (549)	5 (62)	13 (86)
Total	19 (476)	90 (3,994)	25 (265)	112 (441)	9 (372)	71 (2,929)	14 (289)	48 (397)
Percentage AChR-ir	4	2	9	25	2	2	5	12

[1]Numbers of profiles representing each nonsomatic cellular compartment that were labelled for m1 or m2 ACh receptors. Each profile was counted just once, regardless of the density of silver particles within the profile or whether those particles were membrane associated or cytoplasmic. The total number of each type of profile that was encountered is given in parentheses. Because every profile was counted in each image, the sample size for each profile type is different, reflecting the neuropil composition of layers 2 and 3 in V1. The bottom row summarizes the data as percentages of profiles that were immunoreactive, summed across both layers. N = 9,163 identified cellular compartments.

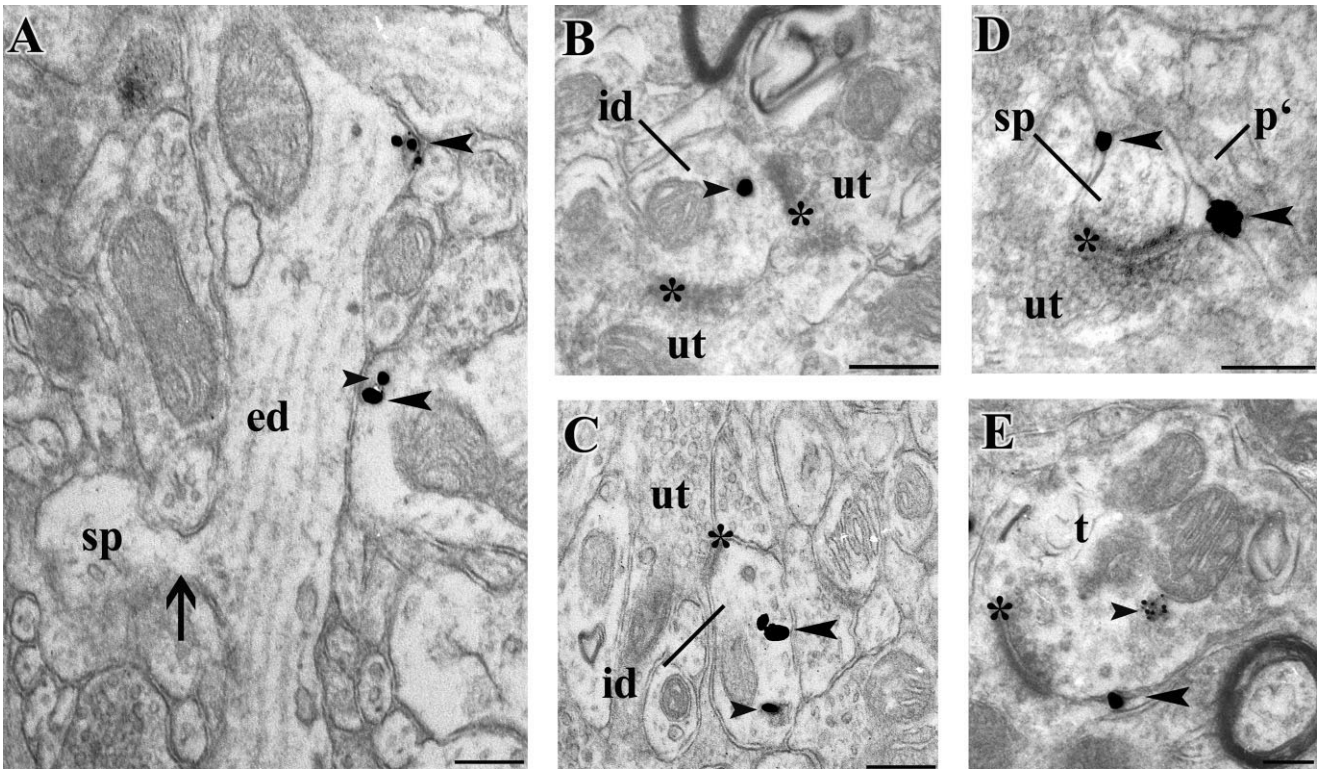

Fig. 8. m1 and m2 AChR immunoreactivity in V1 by EM. ed, mAChR-ir putatively glutamatergic dendrite; id, mAChR-ir putatively GABAergic dendrite; sp, spine head; ut, unlabelled terminal; t, labelled terminal; p, mAChR-ir process; asterisk, asymmetric synapse; large arrowhead, membrane-associated mAChR; small arrowhead, cytoplasmic mAChR; arrow, spine neck. **A** shows an m1 AChR-ir dendrite (ed). This dendrite has a spine (sp) emerging from it, with the spine neck visibly continuous with the dendritic shaft (arrow). This identifies the dendrite as probably belonging to a spiny (glutamatergic) neuron. At the point near the top of the image where a cluster of silver particles is seen (large arrowhead), the dendrite protrudes, indicating another possible spine site. **B** shows another dendrite (id). This dendrite is receiving two direct asymmetric synapses (asterisks), indicating that it is probably part of an aspiny (inhibitory) neuron. The terminals making these synapses are both immunonegative (ut), whereas the dendrite presents a single cytoplasmic silver particle (arrowhead), here indicating m2 AChR immunoreactivity. **C** also shows a putatively inhibitory dendrite (id), again identified by the presence of a direct asymmetric synapse (asterisk). The dendrite is m1 AChR-ir both at the membrane (large arrowhead) and in the cytoplasm (small arrowhead). **D** shows an asymmetric synapse (asterisk) onto a spine (sp). Running along the side of the spine, opposite this synapse, is an m2 AChR-ir process (p). The spine has a membrane-associated silver particle (upper arrowhead), indicating that it too is m2 AChR-ir. **E** shows another terminal (t), making an asymmetric synapse (asterisk). The postsynaptic profile presents an m2 AChR receptor (large arrowhead) just adjacent to the synapse itself. Inside the terminal is a cluster of silver particles on a small ring of membrane (small arrowhead), labelling a group of m2 AChR-ir antigenic sites. Scale bars = 200 nm.

(Fig. 8A). There were only 26 of these among the 838 dendrites counted; 3 of 14 (21%) were m1 AChR-ir, and 2 of 12 (17%) were m2 AChR-ir. This sample is too small for meaningful quantitative analysis but suggests only weak excitatory dendritic expression for both receptors. If we assume that all of the remaining (unclassified) dendrites were glutamatergic, we find that only 27% were m1 AChR-ir (94 of 351) and 12% m2 AChR-ir (39 of 332).

Spine labelling. Insofar as most GABAergic cells are aspinous or sparsely spiny, most spines will be compartments of glutamatergic cells; 9% (25 of 265) spines were m1 AChR immunoreactive, and 5% (14 of 289) were m2 AChR-ir. These values correspond extremely well to the levels of expression by glutamatergic neurons that we estimated above, based on somatic labelling (fewer than 10% of glutamatergic neurons expressing each receptor).

It is impossible without a label for GABA to distinguish inhibitory and excitatory axons, but very few axons and terminals were immunoreactive for either receptor anyway; examples of terminal and axonal labelling are shown in Figure 8D,E. In Figure 8D, an asymmetric synapse onto a spine is shown. Running along the side of the spine, opposite this synapse, is an m2 AChR-ir process. Although there is no way to be certain of the identity of this process, a previous study (Aoki and Kabak, 1992) reported a similar configuration of two terminals surrounding a spine head. In that study, the second terminal was immunoreactive for choline acetyltransferase, identifying it as a cholinergic afferent. The m2 AChR serves as a cholinergic autoreceptor in cortex, so the second process in the current micrograph is probably also a cholinergic afferent in very close apposition to this putatively excitatory synapse. In Figure 8E shows an axon terminal with a group of silver particles clustered in the cytoplasm on a ring of membrane. These may be what Schuh and Mueller (1993) have called "receptor-somes," packaged receptors complete with membrane being trafficked within the neuron. m2 AChR-ir membrane rings were seen quite often in dendrites and in both myelinated and unmyelinated axons. m1 AChR rings were extremely rare in comparison.

Membranous vs. cytosolic localization of mAChRs

Most mAChRs were nonsynaptic, and there was a preferential expression on dendrites, both when membrane-associated and when cytoplasmic silver particles were considered. Because of the uncertainty in localization introduced by uneven silver deposition in the process of intensification of gold labels, a conservative approach was taken to the identification of membrane-associated receptors. For a silver particle to be considered membranous, it had to be overlapping with its compartment's membrane. By this criterion, the majority of the m1 AChR labelling was cytoplasmic; 66.8% of silver particles (on dendrites or axons, 352 of 527 silver particles) in m1 AChR-labelled tissue were cytoplasmically located. m2 AChRs, on the other hand, were mostly membrane-associated, only 39.6% (72 of 182 silver particles) being cytoplasmic.

As noted above, most m1 AChR labelling was dendritic. 56.2% of membranous silver particles indicating m1 AChRs in layer 2 (81 of 144 silver particles) and 61.3% in layer 3 (19 of 31 silver particles) were on dendrites. The same pattern was observed for cytoplasmic silver particles, of which 81.9% in layer 2 (253 of 309 particles) and 69.8% in layer 3 (30 of 43) were on dendrites.

m2 AChR localization was more complex. As noted above and in Table 1, a higher proportion of dendrites was m2 AChR-ir (12%) than axons (2%). However, when the location of individual labels was considered, 80% of the membrane-associated silver particles (88 of 110) were on axons. This contrasted with cytoplasmic labels, only 19.4% of which (14 of 72) were on axons.

High level of detection for GABAergic neurons

Clear interpretation of the dual-labelling experiment depends on a high detection rate for GABAergic and for m1 and m2 AChR-expressing neurons. Dual-label immunofluorescence, as a technique, can produce a high rate of false negatives because of interactions between antibodies. To rule out the possibility of false negatives, first the density of GABA neurons was examined. Two previous groups have quantified GABAergic neurons in V1 of the macaque monkey by using optimized detection protocols and stereological counting methods (Hendry et al., 1987; Beaulieu et al., 1992). One of these studies performed an additional, nonstereological count also using optimized detection (ABC-DAB) that is comparable to our counting technique (Hendry et al., 1987). The authors report that the average number of GABAergic neurons observed per 50-μm-wide column of V1 tissue (across five animals) was 59.6. To allow comparison, we divided each immunofluorescent montage into four 50-μm-wide columns of tissue and, summing across both animals and across tissue processed for m1 and m2 AChR immunoreactivity, calculated the average number of neurons per column. The value obtained in the present study is 62.3 (sd 6.3; range 53–69) GABAergic neurons per 50-μm-wide column of tissue.

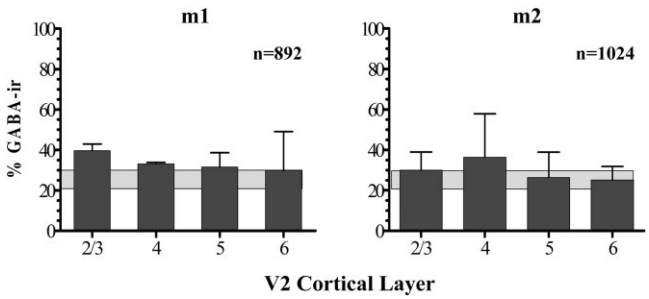

Fig. 9. Dually labelled cells among the mAChR-ir population in V2. These graphs show the percentages of mAChR-ir somata in each layer of V2 that were also immunoreactive for GABA, m1 AChRs on the left, m2 AChRs on the right. The solid line behind the bars indicates the proportions of neurons in V2 that are GABAergic (~25%). It can be seen here that, unlike the case in V1 (Fig. 6), GABAergic neurons are represented among mAChR-expressing neurons in V2 roughly in proportion to their representation in the neuropil in general. N = 1,916; error bars show standard error.

Muscarinic receptors in area V2

There are no previous quantitative studies in macaque V1 concerning the muscarinic population with which to compare our obtained densities for mAChRs. However, early qualitative data from singly labelled tissue visualized by ABC-DAB indicated that area V2 had a higher expression of mAChRs than area V1, and this observation was used to generate an internal control study for mAChR detection.

In the secondary visual cortical area of the macaque, area V2, GABAergic neurons make up approximately 25% of all cortical neurons (Hendry et al., 1987). Dual labelling with antibodies directed against mAChR and GABA showed that 37% of m1 AChR-ir neurons (333 of 892, sd = 7%; *t*-test comparison against 25%, $P = 0.41$) and 35% of m2 AChR-ir neurons (360 of 1,024, sd = 12%; *t*-test comparison against 25%, $P = 0.39$) were GABAergic (Fig. 9). These values are more reflective of the neuropil composition in the area than were the V1 data (compare Figs. 5 and 9). mAChR expression among GABAergic cells was still relatively high; 63% (333 of 527, sd = 1%) expressed m1 AChRs, and 43% (360 of 839, sd = 8%) expressed m2 AChRs. In comparison (by *t*-test) with the V1 data, there were no differences between the two areas in the expres-

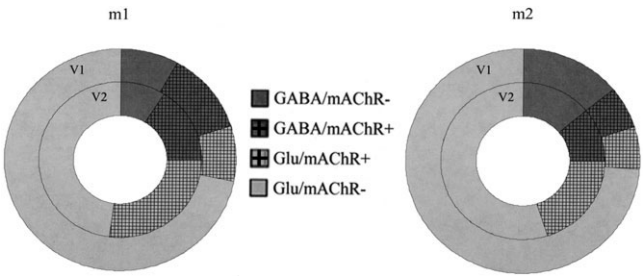

Fig. 10. Estimated mAChR expression by GABAergic and non-GABAergic cells in V1. These donut charts compare our estimates for mAChR expression by GABAergic and glutamatergic neurons in V1 with the estimates for V2. The outer rings represent the data shown in the pie charts of Figure 8. The inner rings show the corresponding values for area V2. In both rings, the dark gray slices represent GABAergic neurons (20% of V1 neurons, 25% in V2) and the pale gray represent glutamatergic neurons (80% in V1, 75% in V2). The textured overlays show the proportion of neurons that were immunoreactive for m1 (left) or m2 (right) AChRs. This makes clear both the increase in expression of both mAChRs in area V2 and the stronger expression by glutamatergic neurons.

sion of m1 ($P = 0.27$) or m2 ($P = 0.13$) mAChRs by interneurons.

Again, by using the above-described percentages to estimate the level of expression in inhibitory and excitatory neurons, 16% of V2 neurons (60% of the GABAergic population, 25% of all neurons) are m1 AChR-expressing interneurons, and this is roughly one-third of the m1 AChR-ir population. Meanwhile, 11% of V2 neurons are m2 AChR-expressing interneurons, which is also about one-third of the m2 AChR-ir population. These numbers indicate that at least 43% of V2 neurons express m1 AChRs (16% of V2 cells being GABAergic cells expressing m1 AChRs and 27% being glutamatergic m1 AChR-expressing cells) and at least 31% express m2 AChRs (11% of V2 neurons being GABAergic m2 AChR-epxressing cells and 20% being glutamatergic and m2 AChR-expressing). The resulting estimates for expression among glutamatergic neurons are double those for V1 (Fig. 10).

Immunoreactivity across V1 subdivisions

Using the FM data set, comparisons were made between the cytochrome oxidase-rich blobs and the cytochrome oxidase-poor interblobs in the upper layers (Wong-Riley et al., 1998). Because the data images were 200 μm across, only the 34 images that were centered on the blob or interblob center (determined from an adjacent reference section; see Materials and Methods) were included in this analysis. Table 2A presents the data on GABA immunoreactivity among mAChR-expressing cells in blobs and in interblobs. Means for the two groups (blob vs. interblobs) were compared by *t*-test, which showed that GABA-ir neurons in blobs were more likely to express m2 AChRs AChRs than were GABA-ir neurons in interblobs ($P = 0.02$). GABA-ir neurons across these two compartments were equally likely to express m1 AChRs ($P = 0.10$), and there was no difference in the size of the dually labelled population or either the m1 AChR-expressing ($P = 0.33$) or the m2 AChR-expressing ($P = 0.10$) cells.

DISCUSSION

We have shown that, although the level of mAChR expression by *GABAergic neurons* is similar in the primary (V1) and secondary (V2) visual areas of the macaque monkey, mAChR expression by *glutamatergic neurons* is much stronger in V2 than in V1. We also found that overall mAChR expression in both areas is quite low. A previous study (Erisir et al., 2001), using different methods (light and electron microscopy), found that interneurons were overrepresented among m2 AChR-ir neurons in cat area 17, but many in vitro physiology experiments suggest that cholinoceptivity is a feature of most glutamatergic neurons in neocortex (McCormick, 1993; McCormick and Prince, 1985, 1986; Wang and McCormick, 1993). Additionally, several anatomical studies using antibodies directed against mAChRs have emphasized labelling of pyramidal neurons (Brann et al., 1993; Chessell et al., 1993; Levey et al., 1991; Mrzljak et al., 1993). In contrast, our results indicate relatively low expression by glutamatergic neurons and high expression among inhibitory interneurons. In light of the differences between our results and those from other groups, we present a number of control studies that support our conclusion.

Antigen detection

Both detection failure and the converse problem of overestimating an immunoreactive population must be considered; either error would undermine the validity of our dual-labelling data. Detection of GABAergic interneurons was excellent, comparable to that of studies that used the ABC-DAB method for visualization (Hendry et al., 1987; Beaulieu et al., 1992). ABC-DAB is very sensitive and is enzymatically amplified and, as such, can be considered a gold standard for detection methods. Thus there is reason to be confident that the data presented neither under- nor overestimate the GABAergic population.

For the mAChRs, there are no previous quantitative studies with which to compare our data. Having reported low levels of mAChR expression, the possibility of detection failure must be considered. This could happen because the mAChR antibodies used might not recognize receptors that are G-protein bound (i.e., those that were recently active) as a result of epitope masking. G-proteins probably bind to mAChRs somewhere on the i3 intracellular loop (Pangalos and Davies, 2002), which is also where the target epitope for both mAChR antibodies is located. However, the i3 loop is large, and, although the precise site of interaction between mAChRs and G-proteins is not well understood, it is known that much of this loop can be deleted from mAChRs without interfering with G-protein binding (Hulme et al., 2001; Schoneberg et al., 1995). This suggests that the G-protein interaction site on the i3 loop of mAChRs is small. Thus, even if a G-protein is bound, it is unlikely that the entire binding epitope for either the m1 or the m2 AChR antibody (each >120 amino acids in length) would be masked. Use of polyclonal antibodies also reduces the risk of detection failure resulting from epitope masking, insofar as the presence of multiple clones increases the probability that at least some will bind to a portion of the i3 loop, no matter what its conformational state. We consider it likely, based on these considerations, that each of these antibodies would offer a high probability of antigen detection.

TABLE 2A GABAergic Neurons Within the mAChR-ir Population: Blob/Interblob Comparison[1]

	Blobs		Interblobs	
	Mean percentage (sd)	Total counts	Mean percentage (sd)	Total counts
m1 AChR	54 (3)	94 of 175 m1-ir neurons	45 (9)	60 of 132 m1-ir neurons
m2 AChR	58 (5)	180 of 308 m2-ir neurons	46 (9)	129 of 280 m2-ir neurons

[1]Immunofluorescence data from layers 2 and 3, subdivided into counts from within blobs and those from the interblob regions. Percentages of mAChR-ir neurons that were GABAergic. The top row shows the number of dually labelled neurons as a percentage of all neurons immunoreactive for m1 AChRs within blobs (left) and interblobs (right). Also presented, in the "raw data" columns are the corresponding numbers from which these percentages were calculated (summed across both animals). The bottom row shows the same data for the population of m2 AChR-ir neurons.

TABLE 2B mAChR Expression in GABAergic Neurons: Blob/Interblob Comparison[1]

	Blobs		Interblobs	
	Mean percentage (sd)	Total counts	Mean percentage (sd)	Total counts
m1 AChR	68 (1)	94 of 138 GABA-ir neurons	55 (4)	60 of 109 GABA-ir neurons
m2 AChR	55 (7)	180 of 333 GABA-ir neurons	31 (8)	129 of 411 GABA-ir neurons

[1]Immunofluorescence data from layers 2 and 3, subdivided into counts from within blobs and those from the interblob regions. Percentages of GABAergic neurons that were m1 AChR-ir (top) or m2 AChR-ir (bottom). The top row shows the number of neurons dually labelled for m1 AChRs and GABA as a percentage of all neurons immunoreactive for GABA within blobs (left) and interblobs (right). The bottom row shows the same data for the proportions of m2 AChR-ir neurons within the GABAergic population.

Detection failures could also occur as a result of interference between antibodies during coincubation. The action of our antibody directed against GABA was clearly not altered in comparison with a single-labelling protocol (as evidenced by our favorable comparison with other, single-labelling studies). However, it is still possible that the mAChR antibodies could be hindered. The V2 data here act as an internal control, because they were collected from the *same tissue sections* as the V1 data; the two are thus identical with respect to processing conditions. The fact that we were able to detect higher levels of expression by glutamatergic neurons in V2 shows that the V1 data are not a result of having reached the detection limit of either the antibodies or the labelling protocol. Where there are more receptors in the tissue, these methods are able to detect them. Thus, our data are most safely viewed as a lower bound on mAChR expression, but they nonetheless show a twofold increase in expression across the V1/V2 border, a change that is specific to glutamatergic neurons.

Somatic labelling as a marker for AChR-ir neurons

Quantifying somatic labelling might have resulted in an underestimate of mAChR expression. This could occur if the receptors are synthesized primarily in dendrites or are made at the soma but rapidly trafficked into the axonal and/or dendritic compartments, resulting in undetectable somatic immunoreactivity in a neuron that actually expresses a protein of interest (see, e.g., Burette et al., 2002). Given that GABA and the two mAChRs might not be precisely colocalized in dendrites or axons, dual immunofluorescence cannot address this question. By using EM instead, we showed that levels of immunoreactivity in nonsomatic compartments (dendrites, spines, axons, and terminals) did not significantly exceed what was predicted by the level of expression in somata. Although examination of the data for any one compartment leaves open the possibility that receptors are being trafficked elsewhere within the cell, our analysis shows that the expressions levels were low across all compartments. The only remaining possibility is that mAChRs were being trafficked to cellular compartments in other layers. Although we performed the complete quantitative analysis only of layers 2 and 3, our EM data montage covered the entire cortical thickness, from pia to white matter. Receptor density did vary from layer to layer, but there was no other layer that appeared to contain a number or distribution of receptors that might alter the conclusions of the current report.

In the EM study, the number of immunoreactive dendrites was compared with the total number of dendrites in layers 2 and 3, and it was found that they were no more frequently labelled than were somata. The most parsimonious explanation for this result is that the somatic count accurately estimates the expression level of m1 and m2 AChRs. However, if mAChR-expressing neurons have thinner dendrites or a shorter total dendritic length (less likely to be encountered in a plane of section), one would not expect the proportion of labelled dendrites to equal that of somata. Qualitatively, the labelled dendrites in our tissue did not differ in diameter from unlabelled dendrites, so it is unlikely that size differences would have led to undersampling of mAChR-ir processes. On the other hand, we have no data, qualitative or quantitative, on the total dendritic length of mAChR-ir neurons in comparison with other cortical cells, so we cannot rule out the possibility that morphological differences contributed to the observed levels of immunoreactivity. It would be interesting if it turned out that mAChR-expressing cells were morphologically distinct; this is an area that warrants further study.

Finally, the low levels of axonal and axon terminal labelling deserve particular mention; they may be due to the fact that many axons in layers 2 and 3 probably arise from neurons whose somata lie in other cortical areas. However, to obtain even the 15–20% estimate for mAChR expression provided by the somatic data, one would have to propose that over 90% of the axons encountered in layers 2 and 3 came from outside V1. As discussed above, the expectation that the proportion of mAChR-ir axons should not exceed that of somata assumes similar total axon lengths for mAChR-ir and mAChR-negative neurons. In the end, because dendrites and axons did not express mAChRs to a greater extent than somata, and because we have no evidence that mAChR-ir neurons represent a distinct morphological class with smaller den-

dritic trees and/or axonal arbors, we conclude that somatic counting did not underestimate the population of mAChR-expressing cells.

A more subtle interpretation of the observed patterns of somatic and nonsomatic immunoreactivity is that GABAergic neurons express mAChRs at the soma (accounting for our somatic data), whereas glutamatergic neurons express mAChRs in their dendrites (and thus account for most, or all, of the nonsomatic labelling). The tissue used for EM analysis was processed as part of another experiment and did not contain a second label for GABA. Instead, morphology was used to investigate whether dendritic expression differed between putatively glutamatergic and GABAergic profiles. There does appear to be a preferential localization of mAChRs to the soma in GABAergic neurons, evidenced by lower-than-expected expression of mAChRs among dendrites receiving direct asymmetric synapses. Although the small number of profiles used in this analysis cautions against drawing strong conclusions from these data, this observation actually strengthens the argument for preferential targeting of mAChR-mediated cholinergic effects to interneurons in V1. Expression of mAChRs at the soma allows for greater access to the final phase of synaptic integration and spike generation, availing the cholinergic system of strong control over the level of the inhibition in V1. Somatic expression for mAChRs on interneurons also places the receptors close to the site of ACh release, insofar as it has been shown that, in cat primary visual cortex, cholinergic terminals are most often juxtaposed to GABAergic somata (Beaulieu and Somogyi, 1991; Erisir et al., 2001).

This leaves the possibility that much of the dendritic labelling observed arose from glutamatergic neurons. However, even if all of the unclassified mAChR-ir dendrites arose from glutamatergic neurons (which is highly unlikely), immunoreactive dendrites still made up less than one-fourth of *all* dendrites encountered. Thus, either very few glutamatergic neurons were expressing mAChRs, as estimated from the analysis of immunofluorescence data, or, if many glutamatergic neurons were expressing mAChRs, then those receptors must be distributed within dendrites very sparsely indeed (at least in layers 2 and 3, where our analysis was focused). In either case, our data support the conclusion of relatively weak modulation of glutamatergic neurons by m1 and m2 receptors in area V1. Finally, there is the possibility that V1 uses the m3, m4, or m5 receptor subtypes in place of m1 and m2. Previous qualitative data suggest that this is not the case; m3 and m4 expression is not particularly high in V1 (Tigges et al., 1997).

Large cytoplasmic pools of m2 AChRs in dendrites

It is also interesting to note from the EM study that, although most m2 AChRs were found on dendrites, and very few axons were labelled, most *membrane-associated* m2 AChRs were on axons. Perhaps the cytoplasmic receptors in dendrites were a "ready pool," whereas the few immunoreactive axons had actually been more actively receptive to ACh release. It is known that neurons in the striatum internalize m2 AChRs after receptor activation, and this internalization triggers degradation, evidenced by the presence of m2 AChR immunoreactivity on multivesicular bodies (Bernard et al., 1998). In the present study, none of the drugs given prior to euthanasia is known to be a muscarinic agonist, and the observed cytoplasmic m2 AChRs were not associated with multivesicular bodies. It seems reasonable to conclude that, at least in the tissue we examined, m2 AChR-mediated modulation may to be more active in labelled axons than in labelled dendrites.

Muscarinic responses in vivo

In guinea pig cingulate cortex in vitro, most excitatory cells respond directly to ACh (McCormick and Prince, 1986). There are, however, no in vitro studies of cholinergic responses in macaque V1. Previous in vivo extracellular recording experiments in cat area 17 reveal that 85–90% of neurons respond to ACh (Muller and Singer, 1989; Stewart et al., 1999), whereas, for the marmoset, studies indicate that only 55% of cells respond to ACh (Roberts et al., 2005). Thus there may be a significant species differences in AChR expression, at least in the primary visual cortices. The alternative explanation would be that the small fraction of somatic and dendritic plasma membrane expressing mAChRs must nevertheless be able to exert global influences (such as membrane depolarization and changes in adaptation) on single cells.

Muscarinic modulation in V1 and V2

In showing that mAChR expression by inhibitory neurons is roughly constant across V1 and V2, whereas expression in glutamatergic neurons varies, our data raise the interesting possibility that ACh mediates distinct and partially separable functions acting through the inhibitory vs. the excitatory networks. Whatever role cholinergic modulation plays when acting on interneurons should be observable in both V1 and V2, whereas another role, mediated by cholinergic action on excitatory cells (or by coordinated modulation of both excitation and inhibition together), will be more evident in V2 than in V1.

Many cognitive tasks have been associated with cholinergic modulation. Perhaps the most clearly demonstrated for neocortex are the links between ACh and attention (for review see Sarter et al., 2005; Yu and Dayan, 2005) and plasticity (for reviews see Edeline, 2003; Gu, 2003; Kilgard, 2003; Rasmusson, 2000). A current model of cholinergic mediation of attention in primary sensory cortices proposes that nicotinic modulation of thalamic terminals enhances ascending input from the thalamus, whereas muscarinic modulation of glutamatergic neurons suppresses lateral spread of excitation within cortex (Gil et al., 1997; Hasselmo and Bower, 1992; Hasselmo and McGaughy, 2004; Hsieh et al., 2000). Our data suggest that the level of expression of mAChRs by glutamatergic neurons in V1 is very low, so it is unlikely that there is significant muscarinic suppression of intracortical synapses in this cortical area. However, we have data showing that, in macaque, thalamic terminals do express nicotinic receptors, allowing for the thalamocortical enhancement that the theory predicts (Disney and Aoki, 2003b).

There are increasing data showing that attentional states are correlated with an increase in γ-band oscillatory activity in neocortical networks, including the visual cortex of monkeys and humans (Fries et al., 2001; Gruber et al., 1999), and that these oscillations are dependant in part on fast-spiking inhibitory neurons (Steriade et al., 1998; Tiesinga et al., 2001, 2004; Traub et al., 1996; Vreugdenhil et al., 2003). It is also known that muscarinic

agonists can alter γ-band activity in visual cortex (Rodriguez et al., 2004). Many fast-spiking interneurons express parvalbumin, both in rodent (Kawaguchi and Kubota, 1993) and in macaque (Zaitsev et al., 2005), and we have preliminary data showing that much of the expression of m1 AChRs in V1 is accounted for by expression in parvalbumin-immunoreactive neurons (Disney and Aoki, 2003a). Perhaps attention requires coordinated modulation of thalamic terminals via nicotinic receptors and of fast-spiking interneurons and glutamatergic neurons via muscarinic receptors. We would then expect that the component of this coordinated modulation that acts via glutamatergic neurons would be very weak in V1. Perhaps this is part of the reason why measured attentional effects are so much weaker in this area. For both macaques and humans, there is evidence that attentional effects are weaker in area V1 than in area V2 and that the strength of attentional modulation continues to increase up through V3, V4, etc. (see, e.g., Luck et al., 1997; Moran and Desimone, 1985; Tootell et al., 1998).

The fact that muscarinic modulation of excitatory cells in macaque V1 is probably relatively weak makes V1 an excellent model system for studying the role of cholinergic modulation of inhibition, insofar as the effect of ACh on inhibition will be relatively stronger in V1 compared with other cortical areas. Such experiments could address not only the cholinergic basis of attention and γ-band activity but also cholinergic modulation of various forms of cortical plasticity that might depend on interneurons as well (see, for example, E.G. Jones, 1993).

ACKNOWLEDGMENTS

The authors gratefully acknowledge the technical support and advice provided by Claudia Farb, Veera Mahadomrongkul, and Sho Fujisawa. We also thank Michael Hawken, Murray Sherman, Nigel Daw, Dan Sanes, Mal Semple, and Max Schiff for helpful comments on earlier versions of the manuscript.

LITERATURE CITED

Aoki C, Kabak S. 1992. Cholinergic terminals in the cat visual cortex: ultrastructural basis for interaction with glutamate-immunoreactive neurons and other cells. Vis Neurosci 8:177–191.

Beaulieu C, Somogyi P. 1991. Enrichment of cholinergic synaptic terminals on GABAergic neurons and coexistence of immunoreactive GABA and choline acetyltransferase in the same synaptic terminals in the striate cortex of the cat. J Comp Neurol 304:666–680.

Beaulieu C, Kisvarday Z, Somogyi P, Cynader M, Cowey A. 1992. Quantitative distribution of GABA-immunopositive and -immunonegative neurons and synapses in the monkey striate cortex (area 17). Cereb Cortex 2:295–309.

Bernard V, Laribi O, Levey AI, Bloch B. 1998. Subcellular redistribution of m2 muscarinic acetylcholine receptors in striatal interneurons in vivo after acute cholinergic stimulation. J Neurosci 18:10207–10218.

Brann MR, Ellis J, Jorgensen H, Hill-Eubanks H, Jones SVP. 1993. Muscarinic acetylcholine receptor subtypes: localization and structure/function. Prog Brain Res 98:121–127.

Burette A, Zabel U, Weinberg RJ, Schmidt HH, Valtschanoff JG. 2002. Synaptic localization of nitric oxide synthase and soluble guanylyl cyclase in the hippocampus. J Neurosci 22:8961–8970.

Chessell IP, Francis PT, Pangalos MN, Pearson RC, Bowen DM. 1993. Localisation of muscarinic (m1) and other neurotransmitter receptors on corticofugal-projecting pyramidal neurones. Brain Res 632:86–94.

de Lima AD, Singer W. 1986. Cholinergic innervation of the cat striate cortex: a choline acetyltransferase immunocytochemical analysis. J Comp Neurol 250:324–338.

DeFelipe J. 1993. Neocortical neuronal diversity: chemical heterogeneity revealed by colocalization studies of classic neurotransmitters, neuropeptides, calcium-binding proteins, and cell surface molecules. Cereb Cortex 3:273–289.

Descarries L, Gisiger V, Steriade M. 1997. Diffuse transmission by acetylcholine in the CNS. Prog Neurobiol 53:603–625.

Disney AA, Aoki C. 2003a. Cholinergic modulation of inhibitory network sub-elements in V1 of the macaque. Program No. POS-167, Proceedings of the Australian Neuroscience Society.

Disney AA, Aoki C. 2003b. Nicotinic, but not muscarinic, acetylcholine receptors are expressed by thalamic afferents and their terminals in layer IVC of macaque V1. Program No. 701.16, Washington DC: Society for Neuroscience, 2003 [online].

Duttaroy A, Gomeza J, Gan JW, Siddiqui N, Basile AS, Harman WD, Smith PL, Felder CC, Levey AI, Wess J. 2002. Evaluation of muscarinic agonist-induced analgesia in muscarinic acetylcholine receptor knockout mice. Mol Pharmacol 62:1084–1093.

Edeline JM. 2003. The thalamocortical auditory receptive fields: regulation by the states of vigilance, learning and the neuromodulatory systems. Exp Brain Res 153:554–572.

Erisir A, Levey AI, Aoki C. 2001. Muscarinic receptor m2R distribution in the cat visual cortex: laminar distribution, relationship to GABAergic neurons, and the efect of cingulate lesions. J Comp Neurol 441:168–185.

Fitzpatrick D, Lund JS, Schmechel DE, Towles AC. 1987. Distribution of GABAergic neurons and axon terminals in the macaque striate cortex. J Comp Neurol 264:73–91.

Fries P, Reynolds JH, Rorie AE, Desimone R. 2001. Modulation of oscillatory neuronal synchronization by selective visual attention. Science 291:1560–1563.

Gil Z, Connors BW, Amitai Y. 1997. Differential regulation of neocortical synapses by neuromodulators and activity. Neuron 19:679–686.

Gruber T, Muller MM, Keil A, Elbert T. 1999. Selective visual-spatial attention alters induced gamma band responses in the human EEG. Clin Neurophysiol 110:2074–2085.

Gu Q. 2003. Contribution of acetylcholine to visual cortex plasticity. Neurobiol Learn Mem 80:291–301.

Hamilton SE, Loose MD, Qi M, Levey AI, Hille B, McKnight GS, Idzerda RL, Nathanson NM. 1997. Disruption of the m1 receptor gene ablates muscarinic receptor-dependent M current regulation and seizure activity in mice. Proc Natl Acad Sci U S A 94:13311–13316.

Han ZY, Le Novere N, Zoli M, Hill JA, Champtiaux N, Changeux JP. 2000. Localization of nAChR subunit mRNAs in the brain of *Macaca mulatta*. Eur J Neurosci 12:3664–3674.

Hasselmo ME, Bower JM. 1992. Cholinergic suppression specific to intrinsic not afferent fiber synapses in rat piriform (olfactory) cortex. J Neurophysiol 67:1222–1229.

Hasselmo ME, McGaughy J. 2004. High acetylcholine levels set circuit dynamics for attention and encoding and low acetylcholine levels set dynamics for consolidation. Prog Brain Res 145:207–231.

Hendry SH, Schwark HD, Jones EG, Yan J. 1987. Numbers and proportions of GABA-immunoreactive neurons in different areas of monkey cerebral cortex. J Neurosci 7:1503–1519.

Hsieh CY, Cruikshank SJ, Metherate R. 2000. Differential modulation of auditory thalamocortical and intracortical synaptic transmission by cholinergic agonist. Brain Res 880:51–64.

Hsu SM, Raine L, Fanger H. 1981. Use of avidin-biotin-peroxidase complex (ABC) in immunoperoxidase techniques: a comparison between ABC and unlabeled antibody (PAP) procedures. J Histochem Cytochem 29:577–580.

Hulme EC, Lu ZL, Bee M, Curtis CA, Saldanha J. 2001. The conformational switch in muscarinic acetylcholine receptors. Life Sci 68:2495–2500.

Jones EG. 1993. GABAergic neurons and their role in cortical plasticity in primates. Cereb Cortex 3:361–372.

Jones SVP. 1993. Muscarinic receptor subtypes—modulation of ion channels. Life Sci 52:457–464.

Kawaguchi Y, Kubota Y. 1993. Correlation of physiological subgroupings of nonpyramidal cells with parvalbumin- and calbindinD28k-immunoreactive neurons in layer V of rat frontal cortex. J Neurophysiol 70:387–396.

Kilgard M. 2003. Cholinergic modulation of skill learning and plasticity. Neuron 38:678–680.

Levey AI, Kitt CA, Simonds WF, Price DL, Brann MR. 1991. Identification

and localization of muscarinic acetylcholine receptor proteins in brain with subtype-specific antibodies. J Neurosci 11:3218–3226.

Linster C, Cleland TA. 2002. Cholinergic modulation of sensory representations in the olfactory bulb. Neural Netw 15:709–717.

Linster C, Maloney M, Patil M, Hasselmo ME. 2003. Enhanced cholinergic suppression of previously strengthened synapses enables the formation of self-organized representations in olfactory cortex. Neurobiol Learn Mem 80:302–314.

Luck SJ, Chelazzi L, Hillyard SA, Desimone R. 1997. Neural mechanisms of spatial selective attention in areas V1, V2, and V4 of macaque visual cortex. J Neurophysiol 77:24–42.

McCormick DA. 1993. Actions of acetylcholine in the cerebral cortex and thalamus and implications for function. Prog Brain Res 98:303–308.

McCormick DA, Prince DA. 1985. Two types of muscarinic response to acetylcholine in mammalian cortical neurons. Proc Natl Acad Sci U S A 82:6344–6348.

McCormick DA, Prince DA. 1986. Mechanisms of action of acetylcholine in the guinea-pig cerebral cortex in vitro. J Physiol 375:169–194.

Mesulam MM, Mufson EJ, Levey AI, Wainer BH. 1983a. Cholinergic innervation of cortex by the basal forebrain: cytochemistry and cortical connections of the septal area, diagonal band nuclei, nucleus basalis (substantia innominata), and hypothalamus in the rhesus monkey. J Comp Neurol 214:170–197.

Mesulam MM, Mufson EJ, Wainer BH, Levey AI. 1983b. Central cholinergic pathways in the rat: an overview based on an alternative nomenclature (Ch1–Ch6). Neuroscience 10:1185–1201.

Metherate R, Weinberger NM. 1989. Acetylcholine produces stimulus-specific receptive field alterations in cat auditory cortex. Brain Res 480:372–377.

Moran J, Desimone R. 1985. Selective attention gates visual processing in the extrastriate cortex. Science 229:782–784.

Mrzljak L, Levey AI, Goldman-Rakic PS. 1993. Association of m1 and m2 muscarinic receptor proteins with asymmetric synapses in the primate cerebral cortex: morphological evidence for cholinergic modulation of excitatory neurotransmission. Proc Natl Acad Sci U S A 90:5194–5198.

Mrzljak L, Pappy M, Leranth C, Goldman-Rakic PS. 1995. Cholinergic synaptic circuitry in the macaque prefrontal cortex. J Comp Neurol 357:603–617.

Mrzljak L, Levey AI, Rakic P. 1996. Selective expression of m2 muscarinic receptor in the parvocellular channel of the primate visual cortex. Proc Natl Acad Sci U S A 93:7337–7340.

Muller CM, Singer W. 1989. Acetylcholine-induced inhibition in the cat visual cortex is mediated by a GABAergic mechanism. Brain Res 487: 335–342.

Pangalos MN, Davies CH, editors. 2002. Understanding G protein-coupled receptors and their role in the CNS. New York: Oxford University Press.

Park PS, Wells JW. 2004. Oligomeric potential of the M2 muscarinic cholinergic receptor. J Neurochem 90:537–548.

Platt ML, Glimcher PW. 1997. Responses of intraparietal neurons to saccadic targets and visual distractors. J Neurophysiol 78:1574–1589.

Rasmusson DD. 2000. The role of acetylcholine in cortical synaptic plasticity. Behav Brain Res 115:205–218.

Rezvani AH, Levin ED. 2001. Cognitive effects of nicotine. Biol Psychiatry 49:258–267.

Roberts MJ, Zinke W, Guo K, Robertson R, McDonald JS, Thiele A. 2005. Acetylcholine dynamically controls spatial integration in marmoset primary visual cortex. J Neurophysiol 93:2062–2072.

Rodriguez R, Kallenbach U, Singer W, Munk MH. 2004. Short- and long-term effects of cholinergic modulation on gamma oscillations and response synchronization in the visual cortex. J Neurosci 24:10369–10378.

Sarter M, Bruno JP, Givens B. 2003. Attentional functions of cortical cholinergic inputs: what does it mean for learning and memory? Neurobiol Learn Mem 80:245–256.

Sarter M, Hasselmo ME, Bruno JP, Givens B. 2005. Unraveling the attentional functions of cortical cholinergic inputs: interactions between signal-driven and cognitive modulation of signal detection. Brain Res Brain Res Rev 48:98–111.

Sato H, Hata Y, Masui H, Tsumoto T. 1987. A functional role of cholinergic innervation to neurons in the cat visual cortex. J Neurophysiol 58:765–780.

Schoneberg T, Liu J, Wess J. 1995. Plasma membrane localization and functional rescue of truncated forms of a G protein-coupled receptor. J Biol Chem 270:18000–18006.

Schuh TJ, Mueller GC. 1993. Estrogen receptor-dependent formation of two distinct multiprotein complexes on the human pS2 gene regulatory segment. Participation of a c-fos related protein. Receptor 3:125–143.

Sillito AM, Kemp JA. 1983. Cholinergic modulation of the functional organization of the cat visual cortex. Brain Res 289:143–155.

Smiley JF, Morrell F, Mesulam MM. 1997. Cholinergic synapses in human cerebral cortex: an ultrastructural study in serial sections. Exp Neurol 144:361–368.

Solomon SG, Peirce JW, Lennie P. 2004. The impact of suppressive surrounds on chromatic properties of cortical neurons. J Neurosci 24:148–160.

Steriade M, Timofeev I, Durmuller N, Grenier F. 1998. Dynamic properties of corticothalamic neurons and local cortical interneurons generating fast rhythmic (30–40 Hz) spike bursts. J Neurophysiol 79:483–490.

Stewart AE, Yan Z, Surmeier DJ, Foehring RC. 1999. Muscarine modulates Ca^{2+} channel currents in rat sensorimotor pyramidal cells via two distinct pathways. J Neurophysiol 81:72–84.

Stone TW. 1972a. Cholinergic mechanisms in the rat cerebral cortex. J Physiol 222:155P–156P.

Stone TW. 1972b. Cholinergic mechanisms in the rat somatosensory cerebral cortex. J Physiol 225:485–499.

Tiesinga PH, Fellous JM, Jose JV, Sejnowski TJ. 2001. Computational model of carbachol-induced delta, theta, and gamma oscillations in the hippocampus. Hippocampus 11:251–274.

Tiesinga PH, Fellous JM, Salinas E, Jose JV, Sejnowski TJ. 2004. Inhibitory synchrony as a mechanism for attentional gain modulation. J Physiol (Paris) 98:296–314.

Tigges M, Tigges J, Rees H, Rye D, Levey AI. 1997. Distribution of muscarinic cholinergic receptor proteins m1 to m4 in area 17 of normal and monocularly deprived rhesus monkeys. J Comp Neurol 388:130–145.

Tootell RB, Hadjikhani N, Hall EK, Marrett S, Vanduffel W, Vaughan JT, Dale AM. 1998. The retinotopy of visual spatial attention. Neuron 21:1409–1422.

Traub RD, Whittington MA, Colling SB, Buzsaki G, Jefferys JG. 1996. Analysis of gamma rhythms in the rat hippocampus in vitro and in vivo. J Physiol 493:471–484.

Turrini P, Casu MA, Wong TP, De Koninck Y, Ribeiro-da-Silva A, Cuello AC. 2001. Cholinergic nerve terminals establish classical synapses in the rat cerebral cortex: synaptic pattern and age-related atrophy. Neuroscience 105:277–285.

Umbriaco D, Watkins KC, Descarries L, Cozzari C, Hartman BK. 1994. Ultrastructural and morphometric features of the acetylcholine innervation in adult rat parietal cortex: an electron microscopic study in serial sections. J Comp Neurol 348:351–373.

Venter JC. 1983. Muscarinic cholinergic receptor structure. Receptor size, membrane orientation, and absence of major phylogenetic structural diversity. J Biol Chem 258:4842–4848.

Vreugdenhil M, Jefferys JG, Celio MR, Schwaller B. 2003. Parvalbumin-deficiency facilitates repetitive IPSCs and gamma oscillations in the hippocampus. J Neurophysiol 89:1414–1422.

Wang Z, McCormick DA. 1993. Control of firing mode of corticotectal and corticopontine layer V burst-generating neurons by norepinephrine, acetylcholine, and 1S,3R-ACPD. J Neurosci 13:2199–2216.

White EL. 1989. Cortical circuits: synaptic organization of the cerebral cortex—structure, function and theory. Boston: Birkhauser.

Wong-Riley M, Anderson B, Liebl W, Huang Z. 1998. Neurochemical organization of the macaque striate cortex: correlation of cytochrome oxidase with Na^+K^+ATPase, NADPH-diaphorase, nitric oxide synthase, and N-methyl-D-aspartate receptor subunit 1. Neuroscience 83:1025–1045.

Wouterlood FG, Jorritsma-Byham B. 1993. The anterograde neuroanatomical tracer biotinylated dextran-amine: comparison with the tracer *Phaseolus vulgaris*-leucoagglutinin in preparations for electron microscopy. J Neurosci Methods 48:75–87.

Wozniak DF, Stewart GR, Finger S, Olney JW. 1989. Comparison of behavioral effects of nucleus basalis magnocellularis lesions and somatosensory cortex ablation in the rat. Neuroscience 32:685–700.

Xiang Z, Huguenard JR, Prince DA. 1998. Cholinergic switching within neocortical inhibitory networks. Science 281:985–988.

Yu AJ, Dayan P. 2005. Uncertainty, neuromodulation, and attention. Neuron 46:681–692.

Zaitsev AV, Gonzalez-Burgos G, Povysheva NV, Kroner S, Lewis DA, Krimer LS. 2005. Localization of calcium-binding proteins in physiologically and morphologically characterized interneurons of monkey dorsolateral prefrontal cortex. Cereb Cortex 15:1178–1186.